Electronic effects of oxygen and vanadium impurities in TiAl

1997 J. Phys.: Condens. Matter 9 9829

(http://iopscience.iop.org/0953-8984/9/45/011)

J. Phys.: Condens. Matter **9** (1997) 9829–9843. Printed in the UK PII: S0953-8984(97)84604-8

Electronic effects of oxygen and vanadium impurities in TiAl

Yi Liu†, Kuiying Chen†, Jinghua Zhang†, Zhuangqi Hu†, Gang Lu‡ and Nicholas Kioussis‡

† State Key Laboratory of Rapidly Solidified Nonequilibrium Alloys, Institute of Metal Research, Chinese Academy of Sciences, 72 Wenhua Road, Shenyang 110015, People's Republic of China

‡ Department of Physics and Astronomy, California State University, Northridge, CA 91330-8268, USA

Received 30 May 1997, in final form 3 September 1997

Abstract. The electronic mechanism of oxygen embrittlement of TiAl and the effect of vanadium on the ductility of TiAl have been investigated by the first-principles LDF DV X_α embedded cluster method. According to the impurity formation energy, oxygen energetically prefers to occupy the Ti-rich octahedral interstitial site in TiAl compared with hydrogen. When O impurity is added to pure TiAl, a strong Ti–O bond forms due to Ti d/O p hybridization while no Al–O bond can be observed. The bonding character between Ti atoms changes from d–d σ type to p–p π type. In V-doped TiAl, V greatly enhanced the intraplanar and interplanar bonds. The *local environmental total bond order* (LTBO) provides a reasonable description of the cohesive properties of the local impurity environment. The O impurity reduces the LTBO and partial LTBO of the pure TiAl, while V improves them greatly. Therefore, O should be regarded as an embrittler, and V as a ductilizer.

1. Introduction

The intermetallic TiAl compound exhibits excellent high-temperature strength and high strength to weight ratio among all prospective aluminides investigated, which makes it attractive for potential structural applications at elevated temperatures [1]. Unfortunately, the poor ductility at room temperature of TiAl hinders further practical applications. Even in fine-grained single-phase γ-TiAl, less than 1% plastic elongation can be measured before fracture [2–4]. To resolve the low-temperature brittleness problem, early studies focused on understanding the deformation behaviour of single-phase γ. Recently, Al-lean alloys containing a small fraction of Ti_3Al (α_2) were found to be significantly more ductile than single-phase alloys. The two-phase alloy concept forms the foundation for the development of current γ-based alloys. The plasticity of the duplex alloys has been attributed to both structural and intrinsic changes [4]. More careful measurements confirm that the high ductility of the duplex structure cannot solely be attributed to grain refinement, and intrinsic factors such as deformation mechanism changes are also involved. In duplex binary alloys, the primary γ grains can deform by slip of the $1/2$ [110] unit dislocations and twinning of the $1/6$ [112] Shockley partials, two deformation modes that are not active in single-phase γ alloys at room temperature. Their activation in duplex structure may be attributed to the presence of α_2, which absorbs interstitial oxygen from γ and modifies its dislocation core structure or stacking fault energy [5, 6]. The oxygen-scavenging effect of α_2 has

0953-8984/97/459829+15$19.50

been confirmed by Uemori *et al* [7]. The nominal oxygen contents in γ-based materials are typically 500–1000 ppm. However, the actual content can be lower in the γ phase of a duplex alloy, since the α_2 second phase tends to absorb oxygen preferentially. The oxygen depletion has been speculated to change the deformation mechanism and increase the ductility [4, 8]. In single-phase γ, interstitial oxygen can be lowered by addition of Er to form oxide [9, 10]. More recent experiments directly indicate that the yield stress increases but room-temperature ductility decreases with oxygen content in alloys [11–14]. The above facts suggest that the investigation of the embrittlement mechanism induced by oxygen is significant both scientifically and technically. We will first determine the oxygen embrittlement of TiAl at electronic level by the first-principles local density discrete variational X_α embedded cluster method (LDF DV X_α), though many theoretical efforts have been devoted to the bulk TiAl or defect systems in TiAl [15–20]. Such an electronic mechanism underlying the oxygen embrittlement will be very helpful to gain insight into the impurity-induced embrittlement of TiAl, which inevitably absorbs oxygen in remelting and heat treatment processes. As an efficient ductilization element in TiAl alloys, vanadium has also been investigated as compared with oxygen. The occupation competition between oxygen and hydrogen, which has crucial effects on the environmental embrittlement, is also discussed in the present study. The methodology and cluster model used here are briefly described in section 2. To identify the interstitial site oxygen occupation preferentially and establish the reference for the comparison with doped cases, we calculate the impurity formation energy and electronic structure of pure TiAl in section 3.1. The O-doped, V-doped and O, V-codoped TiAl systems are investigated with impurity formation energy, electron density, bond order, density of states and orbital occupations in sections 3.2–3.4 respectively. The summary and conclusion are presented finally in section 4.

2. Methodology and cluster model

The self-consistent discrete variational X_α embedded cluster method based on the local density function approximation has been employed to study the energy and electronic structure of TiAl alloys. Detailed discussions of the formalism are presented elsewhere [21–25]. Therefore, only brief descriptions of the computational parameters are given here. The exchange–correlation potential has been adopted in the von Barth–Hedin form [26]. The numerical free-atom basis functions were used to obtain the molecular eigenfunctions as a linear combination of atom orbitals. We have obtained these basis functions by numerically solving the Schrödinger equation for a discrete set of sample points. Matrix elements of the Hamiltonian and overlap operators were calculated by three-dimensional Diophantine numerical integration with 1200 integration points per atom in the present calculations. We select 1s–4p for Ti and V, 1s–3d for Al and 1s–3s for O atom as the basis sets respectively. The exterior crystal potential floor V_F has been chosen as E_f [22]. The self-consistent iteration was continued until the Mulliken orbital populations [27] were converged to $<10^{-4}$ e.

γ-TiAl has a face-centred tetragonal (fct) $L1_0$ crystal structure with alternation (002) planes of Ti and Al atoms. The tetragonality is chosen as the experimental value 1.02 Å, with a and c being 3.99 and 4.07 Å respectively [28]. The cluster model $Ti_{20}Al_{20}X$, selected from [20], is presented in figure 1. It has been proved that the size of this cluster is large enough to eliminate the surface effect for inner atoms. In addition, the cluster was embedded into the exterior crystal containing more than 400 atoms in the present work, which makes the results more reasonable than before. Inequivalent atoms in the cluster are denoted by numerical labels (enclosed in parentheses), depending on the D_{4h}

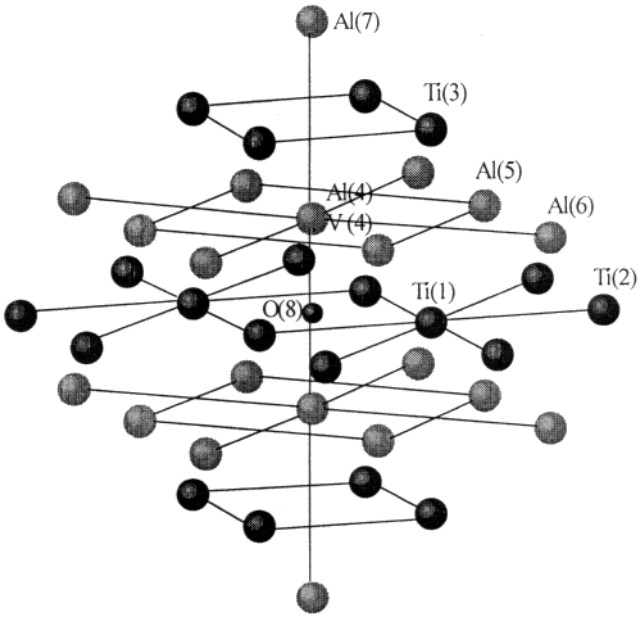

Figure 1. Cluster model used in the calculation. The black, grey and smaller black spheres represent Ti, Al (or V) and O atoms respectively.

point group symmetry. The oxygen atom is placed in the octahedral interstitial site and the vanadium atoms substitute Al(4) atoms in dopant systems. This is based on the experimental evidence that the ductility elements substitute for Al atoms in TiAl [29, 30]. Then, the $Ti_{20}Al_{20}$, $Ti_{20}Al_{20}O$, $Ti_{20}Al_{18}V_2$ and $Ti_{20}Al_{18}V_2O$ clusters are used to simulate the dopant-free, O-doped, V-doped and O, V-codoped TiAl systems respectively. The binding energy, electron density, bond order, density of states and Mulliken orbital populations of the above systems are calculated and analysed in the present work.

3. Numerical results and discussion

3.1. Electronic structure of TiAl

To identify the interstitial site the oxygen atom prefers to occupy, we calculate the impurity formation energy (IFE) as follows:

$$\begin{aligned}\Delta E_{imp} &= E_{tot}(Ti_{20}Al_{20}O) - E_{tot}(Ti_{20}Al_{20}) - E_{tot}(O) \\ &= \{E_{tot}(Ti_{20}Al_{20}O) - [20E_{tot}(Ti) + 20E_{tot}(Al) + E_{tot}(O)]\} \\ &\quad -\{E_{tot}(Ti_{20}Al_{20}) - [20E_{tot}(Ti) + 20E_{tot}(Al)]\} \\ &= E_b(Ti_{20}Al_{20}O) - E_b(Ti_{20}Al_{20}) \qquad (1)\end{aligned}$$

where $E_{tot}(Ti_{20}Al_{20}O)$ and $E_{tot}(Ti_{20}Al_{20})$ are the total energies of the O-doped and dopant-free clusters. $E_{tot}(Ti)$, $E_{tot}(Al)$ and $E_{tot}(O)$ are the total energies of an isolated Ti, Al and O atom respectively. $E_b(Ti_{20}Al_{20}O)$ and $E_b(Ti_{20}Al_{20})$ are the binding energies of the corresponding clusters.

Both Ti-rich and Al-rich octahedral interstitial sites can be obtained when Ti and Al atoms are exchanged in the $Ti_{20}Al_{20}$ cluster. That is, when the black and grey spheres

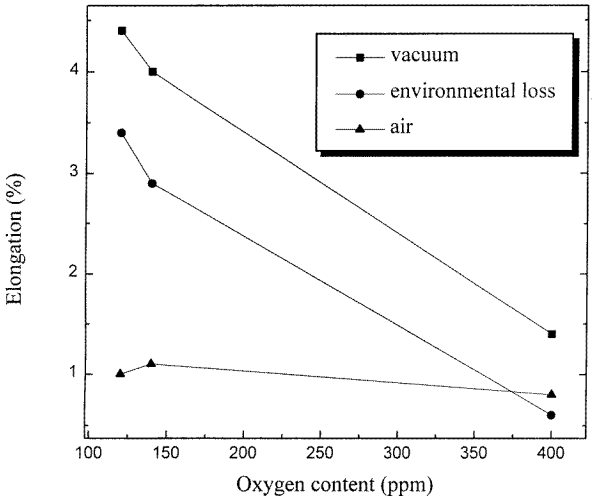

Figure 2. Elongation variation with the oxygen content in Ti–50Al alloy tested in vacuum and air respectively. Environmental loss is defined as the difference of elongation between in vacuum and in air. The experimental data are selected from [14] and replotted here.

represent Ti and Al atoms respectively (figure 1), the octahedral interstitial site is referred to as Ti rich. Vice versa, it is referred to as Al rich. When an O atom is placed into the Ti-rich octahedral environment, the impurity formation energy is 8.04 eV/atom, which is obviously larger than that of the Al-rich case 5.76 eV/atom. This manifests that the O atom is energetically favourable to occupy the Ti-rich octahedral interstitial site rather than the Al-rich one. Therefore, the electronic structure has been studied only when an O atom is placed into the Ti-rich octahedral interstitial site. In our previous work [31], the IFE of hydrogen is 3.99 eV/atom in a Ti-rich environment, while 3.37 eV/atom in an Al-rich environment. These results show that both the oxygen and hydrogen are energetically favourable to occupy the Ti-rich octahedral environment in TiAl. Oxygen has a stronger occupation tendency compared with hydrogen. That is, oxygen prefers to occupy the interstitial site during site competition when both oxygen and hydrogen exist. Oxygen in TiAl can effectively suppress the hydrogen permeation. Moreover it is demonstrated that hydrogen induces environment embrittlement [31, 32]. Then we conclude that the higher the oxygen content in TiAl, the less sensitive to the environmental loss in ductility caused by hydrogen. This conclusion successfully explains the recent experimental results obtained by Wang [14]. The latter author investigated Ti–50Al alloy with three different oxygen content levels, that is, commercial purity (400 ppm), medium purity (140 ppm) and high purity (120 ppm) for their microstructure characters and mechanical properties. Tensile tests in vacuum show that the room-temperature ductility decreases dramatically with the increasing oxygen content (figure 2). Before further discussing the mechanism underlying the oxygen embrittlement, we note that the ductility tested in air is not as sensitive with oxygen content as that in vacuum. The maximum ductility occurs at medium purity level. Environmental loss (EL) is defined as the difference of elongation between in vacuum and in air, which is mainly caused by hydrogen-induced embrittlement [32]. The hydrogen embrittlement of TiAl had been confirmed experimentally [32] and theoretically [31] before. EL decreases obviously with oxygen content, which suggests that the higher-oxygen-content alloy becomes less sensitive to the environment. In fact this anomalous

behaviour in air compared with that in vacuum is the result of the occupation competition between oxygen and hydrogen. At high oxygen content, the oxygen-induced embrittlement mainly contributes to the low ductility. Meanwhile, the EL is the smallest because the oxygen suppresses the hydrogen permeating into the alloy. When oxygen content reduces to the lowest level (120 ppm), hydrogen very easily enters into the alloy. The hydrogen-induced EL (0.5%) is larger than the ductility improvement (0.4%) caused by the decrease of oxygen. The hydrogen-induced embrittlement is dominantly responsible for the lower elongation in this case. We approximately consider the impurity-induced ductility loss composed of oxygen-induced (OL) and hydrogen-induced (HL) parts. In high-oxygen-content TiAl, OL dominantly contributes the ductility loss. If oxygen content reduces to a low level, HL should be mainly responsible for the poor ductility. Other interstitial impurities such as nitrogen and carbon may have a similar behaviour to oxygen. They are present in the amounts of 20–50 ppm and 5–20 ppm respectively and may form nitrides and carbides in single-phase γ materials. So their effects on ductility may be not as strong as oxygen. Consequently, how to avoid or reduce the impurity-induced ductility loss is very crucial for materials scientists to develop new alloys.

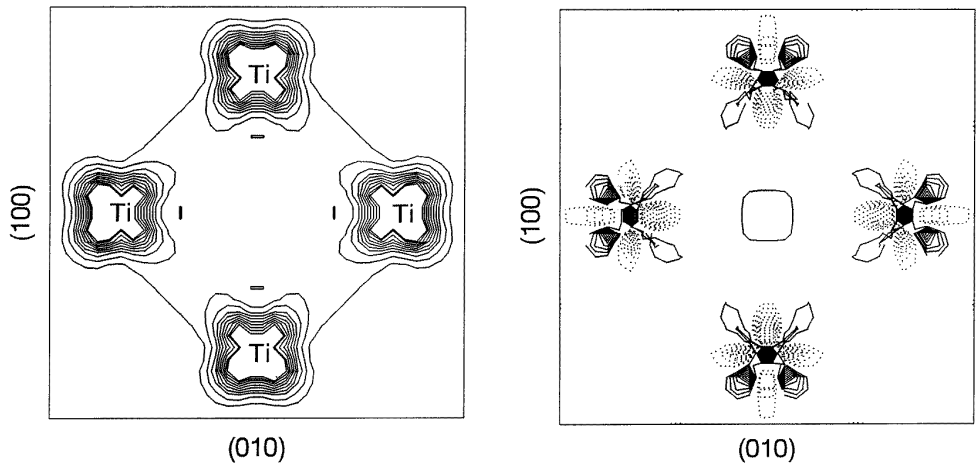

Figure 3. (a) Total electron density in the (002) pure Ti layer of pure TiAl. Contours start from 3.0×10^{-2} e au^{-3} and increase successively by 1.2×10^{-2} e au^{-3}. (b) Bonding charge density in the (002) Ti layer of pure TiAl. Contours start from 1.3×10^{-2} e au^{-3} and increase (decrease) successively by 7.0×10^{-3} e au^{-3}. The solid and dotted contours denote contours of increased and decreased density respectively.

The electronic charge density of pure TiAl has been plotted in figures 3 and 4 for comparison with doped systems. The total electron density of the (002) Ti layer (figure 3(a)) presents the obvious anisotropic electron density, which arises from the strong directional d–d bonding between the first-nearest-neighbour Ti atoms. This can be confirmed by the bonding charge density shown in figure 3(b). The charge around Ti sites accumulates along the first-nearest-neighbour (FNN) direction while it is depleted along the second-nearest-neighbour (SNN) direction. This anisotropic electron distribution induced by d–d Ti bonding must be linked to the brittleness of TiAl [17–20, 33]. The total electron density of the (020) plane is shown in figure 4. The strong Ti d/Al p hybridization character can be found, which agrees well with other theoretical results [17–19].

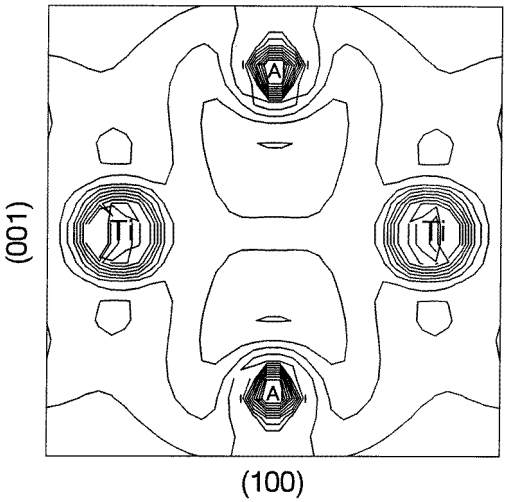

Figure 4. Total electron density in the (020) plane of pure TiAl. Contours start from 1.0×10^{-3} e au^{-3} and increase successively by 1.0×10^{-2} e au^{-3}.

3.2. Effect of oxygen in TiAl

In order to investigate the spatial redistribution of electrons induced by impurity, we calculated the difference electron density by subtracting the superimposed electron density of pure TiAl from the corresponding doped system. For example,

$$\Delta\rho = \rho(\mathrm{Ti_{20}Al_{20}O}) - \rho(\mathrm{Ti_{20}Al_{20}}). \tag{2}$$

The difference electron densities within (002) and (020) planes between O-doped and pure systems are shown in figure 5. Strong electron accumulation can be found in the region between O and Ti(1) atoms, indicating the formation of a strong Ti–O bond (figure 5(a)). On the other hand the depletion between O and Al(4) atoms suggests that a nonbonding state exists between them (figure 5(b)). Bond order calculations show that Ti d/O p hybridization dominantly contributes to the strong Ti–O bonding, while weak Al p/O s, p hybridization combining with the Al s/O s, p antibonding results in the much weaker Al–O bond. Therefore, the bonding between O and the surrounding metal atoms shows significant spatial anisotropy, that is, the stronger lateral O–Ti(1) bonding and much weaker vertical O–Al(4) bonding. It should be noted that the situation is very different in H-doped TiAl [31]. When hydrogen replaces oxygen atoms, an H–Al(4) bond forms while no bond exists between H and Ti(1) atoms.

Significant anisotropic electron redistribution is seen around Ti(1) atoms (figure 5(a)). The charge depletion at the Ti site is along the FNN Ti–Ti direction while accumulation is along the SNN Ti–Ti direction. Compared with the bonding directionality in pure TiAl (figure 3(b)), the d–d σ bonding character between FNN Ti atoms is markedly reduced due to O addition. Meanwhile, the Ti p/Ti p π bonding is greatly enhanced. This change can be confirmed by the bond order (BO) results shown in figure 6. The BO between d orbitals decreases greatly while that between p orbitals increases by the influence of the O impurity. The positive contribution to the Ti–Ti bond from the enhanced p–p π bond cannot compensate the negative effect resulting from the weakened d–d σ bond because the electron cloud overlap between p orbitals is not as strong as that between d orbitals. As a

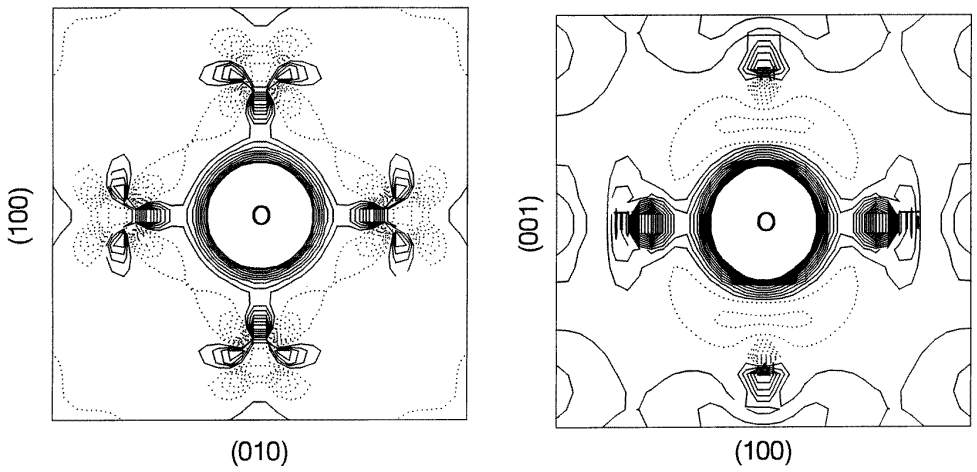

(a) (b)

Figure 5. (a) Difference electron density in the (002) pure Ti layer between O-doped and pure TiAl. Contours start from 1.0×10^{-2} e au^{-3} and increase (decrease) successively by 1.0×10^{-2} e au^{-3}. (b) Difference electron density in the (020) plane between O-doped and pure TiAl. Contours start from 5.0×10^{-3} e au^{-3} and increase (decrease) successively by 6.7×10^{-3} e au^{-3}. The solid and dotted contours denote contours of increased and decreased density respectively.

Table 1. Mulliken orbital populations of pure TiAl, O-doped, V-doped and O, V-codoped TiAl.

	$Ti_{20}Al_{20}$	$Ti_{20}Al_{20}O$		$Ti_{20}Al_{18}V_2$		$Ti_{20}Al_{18}V_2O$	
Atom orbitals	q	q	Δq	q	Δq	q	Δq
Ti(1) 3d	2.1623	2.0124	−0.1508	2.1355	−0.0277	2.0186	−0.1446
4s	0.3509	0.3862	0.0353	0.4014	0.0505	0.4125	0.0616
4p	0.1858	0.3323	0.1465	0.3107	0.1249	0.3937	0.2079
val.	2.6999	2.7309	0.0310	2.8476	0.1477	2.8248	0.1249
Al(4) 3s	1.2264	1.3308	0.1044				
3p	1.5920	1.7444	0.1524				
3d	0.5449	0.0000	−0.5449				
val.	3.3633	3.0752	−0.2881				
V(4) 3d				3.2422		3.3828	0.1406
4s				0.7663		0.6214	−0.1449
4p				0.9384		0.7984	−0.1400
val.				4.9469		4.8026	−0.1443
O(8) 2s		1.5532				1.5746	0.0214
2p		4.8491				4.8449	0.0008
3s		0.3872				0.3270	−0.0602
val.		6.7895				6.7515	−0.0380

result, the BO between Ti(1) atoms reduced, which suggests that O impurity weakens the interaction between Ti atoms. Further Mulliken population analysis (table 1) shows that the charge depletion at the 3d orbital (−0.1508) is nearly equal to the charge accumulation at the 4p orbital (0.1465), while the small total charge increases mainly from the 4s orbital. This clearly shows that the O-induced electron redistribution around Ti(1) atoms is charge

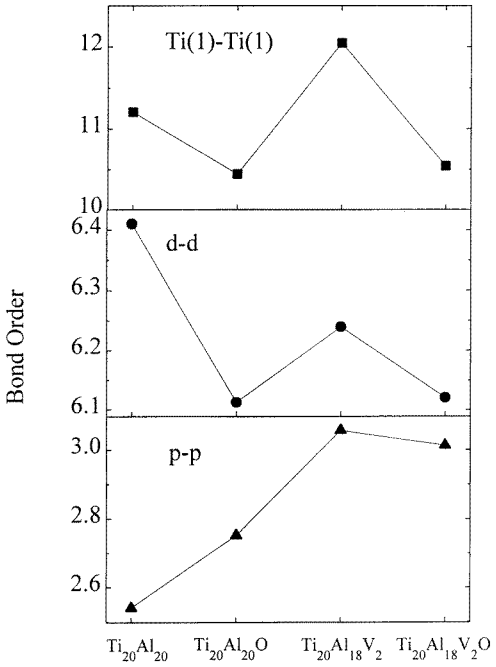

Figure 6. Bond orders between Ti(1) atoms or orbitals in pure and O-doped, V-doped and O, V-codoped TiAl.

transfer from the 3d to 4p orbital, while the total charges increase little. From figure 5(b) the charge depletion also can be seen between Ti(1) and Al(4) atoms. The BO between them decreases from 0.072 in the pure TiAl system to −0.027 in the O-doped case. These results manifest that the strong Ti d/Al p hybridization in pure TiAl was weakened greatly due to oxygen impurity.

Briant and Messmer [34–36] developed the following electronic model to explain the impurity-induced embrittlement of grain boundaries. If the impurity causes embrittlement, the impurity–metal bond will be heteropolar because the impurity will be electronegative with respect to the metal. Charge will be drawn off the metal onto the impurity, leaving less charge to participate in the metal–metal bond. These bonds are consequently weakened. The more electronegative the impurity with respect to the metal, the greater the amount of embrittlement. However, the BM model is not always supported by other calculations. Wu *et al* [37] investigate the effects of phosphorus and boron impurities on the energy and electronic properties of both an iron grain boundary (GB) and its corresponding intergranular fracture surface. Their results show that GB enhancer B results in more charge removal at the surrounding Fe atoms than GB embrittler P. In our calculation on the impurity effects on the Ni/Ni_3Al interface cohesion [38], both the charge obtained by the impurity and the surrounding Ni–Ni bonding strength decrease in the same order, B, C, N, O. These results suggest that the impurity electronegativity with respect to the metal and the loss of charge at the surrounding metal atoms do not appear to be the essential features of impurity-induced embrittlement behaviour. Therefore, we further developed the new electronic model for the impurity-induced embrittlement [38]. Generally, when impurity atoms reside in the interstitial sites in bulk or defect systems, the impurity–metal bond forms and the surrounding metal–metal bond is changed. The impurity-induced metal–metal interaction

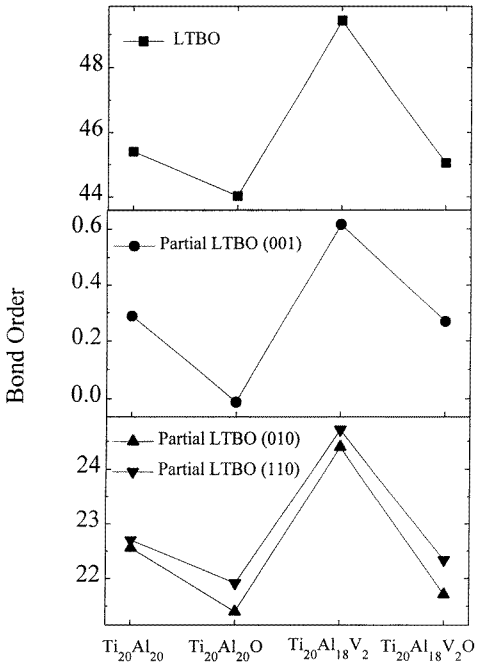

Figure 7. Local environmental total bond order (LTBO) and partial LTBO of (001), (010) and (1,1,0) cleavage planes in pure, O-doped, V-doped and O, V-codoped TiAl.

change is caused not only by the total charge accumulation or depletion, but also the charge transfer and redistribution among atom orbitals. To quantitatively describe this impurity induced cohesion change, we developed a new concept, *local environmental total bond order* (LTBO), which is defined as the sum of all metal–metal and impurity–metal bond orders involved in a local impurity environment, such as an impurity FNN octahedron. A larger LTBO indicates stronger cohesion and better ductility of the system. Our previous work [38] demonstrates that the LTBO is reasonable in estimating the cohesive properties of the local impurity environment. In the present paper, the impurity FNN octahedron is chosen as the local impurity environment. The calculated LTBOs for pure and doped TiAl are presented in figure 7. The LTBO of clean octahedron decreases due to O addition, which shows the oxygen decohesion effect on the local environment. It should be noted that although the total charge of the Ti(1) atom increases slightly (table 1), the Ti–Ti interaction is still weakened (figure 6). This result seems not to be interpreted by the BM model. In fact, according to our new model, it is the charge transfer from d to p orbitals that results in the weaker Ti–Ti interaction, which can be properly indicated by the Ti–Ti BO and LTBO. To investigate the cleavage fracture properties of the local environment, we calculate the partial LTBO of the presumed possible cleavage plane (figure 7), which presents the cleavage strength by summing all broken metal–metal and impurity–metal bond orders. The partial LTBOs of all cleavage planes reduce because of the additive O impurity, which confirms the O embrittlement again. Note that the partial LTBO of the (001) plane is much smaller than that of (010) and (110) planes. It suggests that the (001) plane is the weakest cleavage plane in TiAl material. It is well demonstrated that the Ti d/Ti d directional bonding is among the factors responsible for the poor ductility of γ-TiAl [17–20, 33]. However, it also should be

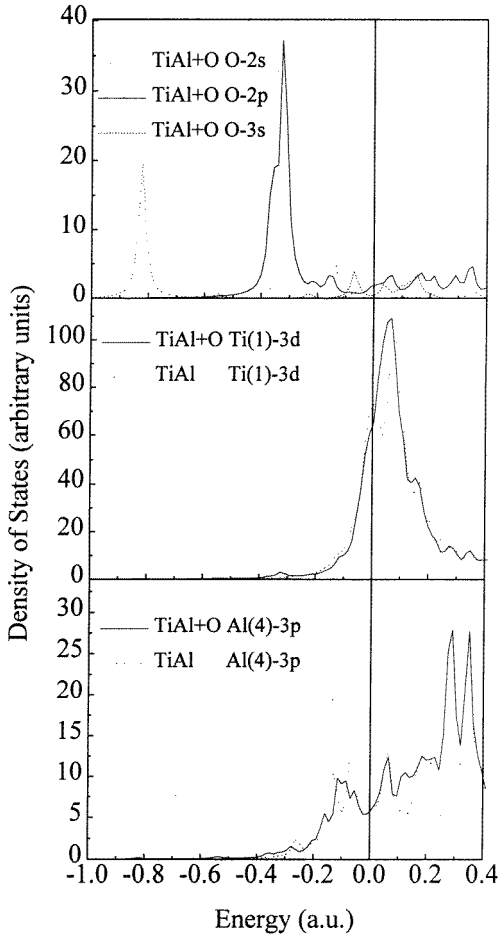

Figure 8. Comparison of the partial DOS of O-doped TiAl with that of pure TiAl. The vertical line represents the location of Fermi energy E_f.

noted that d–d anisotropic bonding is not the only factor indicating the embrittlement. In the present work, although the Ti d/Ti d interaction was weakened due to O impurity (figure 6), the Ti d/O p hybridization provides new bonding anisotropy in the Ti layer. The formation of the Ti–O bond may restrict the motivation of the $1/2$ [110] dislocation. Therefore, the impurity–metal interaction must be involved to properly understand the impurity-induced embrittlement. The LTBO concept includes such impurity–metal interaction, so it provides a sound estimation of the local environment cohesion.

The comparison of the partial DOS of O-doped TiAl with that of pure TiAl is seen in figure 8. It is found that the overlap between Ti(1) 3d and Al(4) 3p peaks reduces because of the O addition. This shows that the Ti d/Al p hybridization was weakened due to the O impurity, which is consistent with the charge depletion (figure 5(b)) and BO drop between Ti(1) and Al(4) atoms. Although the charge at the Ti(1) 3d orbital decreases (table 1), the new small peak about -0.33 au below E_f confirms the formation of a Ti–O bond dominated by Ti d/O p hybridization. The smaller overlap between the Al(4) 3p and O s, p peaks indicates the weaker Al p/O s, p hybridization. These partial DOS results support the

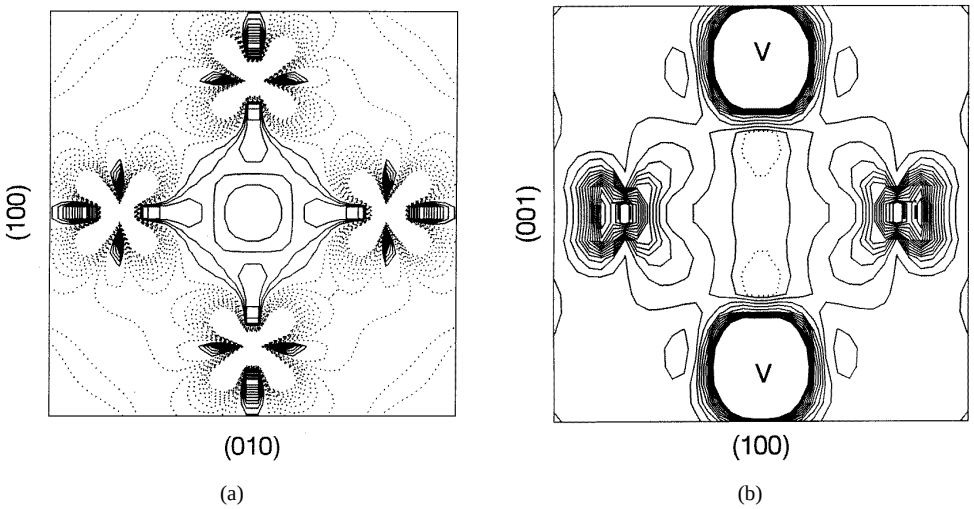

Figure 9. (a) Difference electron density in the (002) pure Ti layer between V-doped and pure TiAl. Contours start from 1.0×10^{-3} e au^{-3} and increase (decrease) successively by 1.0×10^{-3} e au^{-3}. (b) Difference electron density in the (020) plane between V-doped and pure TiAl. Contours start from 1.0×10^{-3} e au^{-3} and increase (decrease) successively by 3.3×10^{-3} e au^{-3}. The solid and dotted contours denote contours of increased and decreased density respectively.

fact that the Ti–O bond is stronger than the Al–O bond according to the BO and electron density contour map (figure 5).

3.3. Effect of vanadium in TiAl

The bonding change due to V substitution for Al atoms is studied by the difference electron density in (002) and (020) planes (figure 9). Remarkable anisotropic electron redistribution is seen around the Ti atoms in the (002) plane. The charge accumulation along the SNN direction shows the strengthened p–p π bond, while the charge depletion along the FNN direction indicates the weakened d–d σ bond. This is supported by the result that BO_{p-p} increases while BO_{d-d} decreases (figure 6). Mulliken populations show that the charge removal at the d orbital in V-doped TiAl is smaller than that of the O-doped case. The charge accumulation at the p orbital mostly comes from the total charge increase. Comparatively, the charge transfer from d to p orbital is the main characteristic in O-doped TiAl. Consequently, the greatly enhanced p–p interaction and not much weakened d–d interaction result in the large Ti–Ti BO. This manifests that the substitution of V strengthens the Ti–Ti bond within the (002) plane compared with the pure TiAl. Note that V addition weakens the d–d directional bonding and no new anisotropic impurity–metal bond forms like the O–Ti bond, which is similar to Mn-doped TiAl [31]. The LTBO and partial LTBO all increase obviously due to V additions, which suggests that V positively contributes to the local environment cohesion. As can be seen in figure 9(b), the charge accumulation at the region between Ti(1) and V(4) atoms indicates that the Ti–V bond is much stronger than the Ti–Al bond in pure TiAl. The high Ti–V and Ti–Ti BO both contribute to the large LTBO. So vanadium should be regarded as an enhancer that is beneficial for the ductility of TiAl.

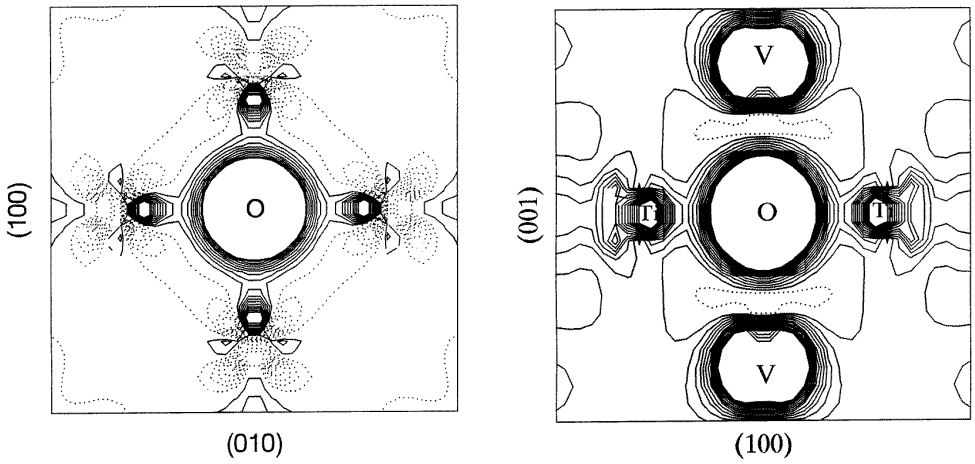

Figure 10. (a) Difference electron density in the (002) pure Ti layer between O, V-codoped and pure TiAl. Contours start from 1.0×10^{-2} e au^{-3} and increase (decrease) successively by 1.0×10^{-2} e au^{-3}. (b) Difference electron density in the (020) plane between O, V-codoped and pure TiAl. Contours start from 5.0×10^{-3} e au^{-3} and increase (decrease) successively by 6.7×10^{-3} e au^{-3}. The solid and dotted contours denote contours of increased and decreased density respectively.

3.4. Effect of oxygen and vanadium in TiAl

To investigate the interaction between impurities having contrasting effects on ductility, we placed the oxygen atom into the octahedron and substituted Al atoms with V atoms. The difference electron densities in (002) and (020) planes are plotted in figure 10. The large charge accumulation between Ti(1) and O atoms indicates the Ti–O bond formation, which shows that the Ti atom still has a strong tendency to combine with O in this case. V d/O p hybridization causes the V–O bond to be stronger than Al–O but weaker than Ti–O. The Ti d–d interaction was reduced while the p–p interaction was strengthened. This also can be concluded by the decreased BO_{d-d} and increased BO_{p-p} (figure 6). According to Mulliken populations (table 1), the large charge transfer from d to p orbital induced by O must be responsible for the reduced d–d interaction. Meanwhile, V additions cause the total charge and p electron rising. As a result, the Ti–Ti bonding is strengthened compared with that of O-doped TiAl, but weakened compared with that of V-doped TiAl. The strong Ti d/V d hybridization greatly favours the interplanar bonding. Comparatively, the Ti d/Al p interaction is markedly weakened when only O is added. The partial DOSs of the V-doped and O, V-codoped TiAl (figure 11) support the above results. The overlap between Ti(1) and V(4) 3d peaks reduced when O impurity was added to V-doped TiAl, which suggests that the strong Ti d/V d hybridization is weakened due to the O impurity. The new peaks about -0.33 au below E_f of Ti(1) and V(4) 3d confirm the Ti, V d/O p hybridization effect. The LTBO and partial LTBO are larger than those in O-doped TiAl but smaller than V-doped TiAl. These facts can be explained by the different contributions from the O and V, which have contrasting effects on the ductility of TiAl. Overall, vanadium can suppress the oxygen-impurity-induced embrittlement by strengthening the interplanar and intraplanar bonding.

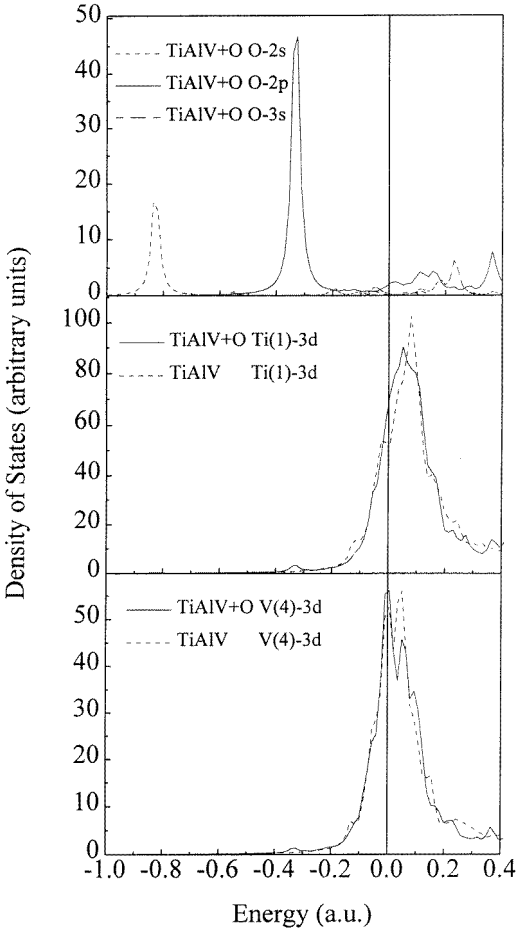

Figure 11. Comparison of the partial DOS of O, V-codoped TiAl with that of the V-doped TiAl. The vertical line represents the location of Fermi energy E_f.

4. Summary and conclusion

The first-principles LDF DV X_α embedded cluster method has been employed to investigate the energy and electronic structure of pure, O- or/and V-doped TiAl. According to the impurity formation energy, oxygen energetically prefers to occupy the Ti-rich octahedral interstitial site in TiAl compared with hydrogen. Then higher-oxygen-content TiAl is less sensitive to the environmental loss in ductility caused by hydrogen. In TiAl with commercial oxygen content, the oxygen-induced ductility loss mainly contributes to the embrittlement. When the oxygen impurity reduces to a very low level, the hydrogen-caused ductility loss should be mostly responsible for the poor ductility. When O impurity is added to pure TiAl, the strong Ti–O bond forms due to Ti d/O p hybridization while no Al–O bond can be observed. The bonding character between Ti atoms changes from d–d σ type to p–p π type. Both the Ti–Ti and Ti–Al bonds are weakened due to the O impurity. In V-doped TiAl, the greatly enhanced p–p interaction and not much weakened d–d interaction result in the strengthened Ti–Ti bond. The Ti–V bond is much stronger than the Ti–Al bond

due to Ti d/V d hybridization. That is, V greatly enhances the intraplanar and interplanar bond. When both O and V exist, the Ti, V d/O p hybridization causes the Ti–O and V–O bond formation. The O-weakened Ti d/Al p interaction in O-doped TiAl can be replaced by the strong Ti d/V d hybridization due to V addition. The *local environmental total bond order* (LTBO) provides a reasonable description of the cohesive properties of the local impurity environment. The O impurity reduces the LTBO and partial LTBO of the pure TiAl, while V improves them greatly. Therefore, O should be regarded as an embrittler that has a decohesion effect, and V as a ductilizer which positively contributes to the local environment cohesion. When both O and V are added, the LTBO and partial LTBO are larger than those in O-doped TiAl but smaller than V-doped TiAl. These facts can be explained by the different contributions from the O and V, which have contrasting effects on the ductility of TiAl. We can conclude that V may suppress the O-impurity-induced embrittlement by strengthening the interplanar and intraplanar bonding. Overall, the above results are consistent with other calculations and related experiments. These must be very helpful to gain an insight into the electronic mechanism of the oxygen embrittlement of TiAl.

Acknowledgments

The authors are very grateful to Dr Deding Wang for providing part of the experimental data. The sponsorship of this research by the National Natural Science Foundation of the People's Republic of China is gratefully acknowledged.

References

[1] Huang S C and Chesnutt J C 1994 *Intermetallic Compounds* vol 2, ed J H Westbrook and R L Fleischer, p 73
[2] McAndrew J B and Kessler H D 1956 *J. Met.* **8** 1348
[3] Shechtman D, Blackburn M J and Lipsitt H A 1974 *Metall. Trans.* **5** 1373
[4] Huang S C and Hall E L 1991 *Metall. Trans.* A **22** 427
[5] Hall E L and Huang S C 1989 *J. Mater. Res.* **4** 595
[6] Vasudevan V K, Court S A, Kurath P and Fraser H L 1989 *Phil. Mag.* **59** 299
[7] Uemori R, Hanamura T and Morkawa H 1992 *Scr. Metall. Mater.* **26** 969
[8] Kawabata T, Tadano M and Izumi O 1988 *Scr. Metall.* **22** 1725
[9] Vasudevan V K, Court S A, Kurath P and Fraser H L 1989 *Scr. Metall.* **23** 467
[10] Sriram S, Vasudevan V K and Dimiduck D M 1991 *Mater. Res. Soc. Symp. Proc.* vol 213 (Pittsburgh, PA: Materials Research Society) p 375
[11] Kawabata T, Abumiya T and Izumi O 1992 *Acta Metall. Mater.* **40** 2557
[12] Murata Y, Morinaga M and Takeda Y 1992 *Mater. Trans.* **33** 419
[13] Yamauchi S and Shiraish H 1992 *Mater. Sci. Eng.* A **152** 283
[14] Wang D 1995 *PhD Thesis* Shanghai Jiaotong University
[15] Anisimov V I, Ganin G V, Galakhov V R and Kurmayev E Z 1987 *Phys. Met. Metall.* **63** 192
[16] Chubb S R, Papaconstantopoulous D A and Klein B M 1988 *Phys. Rev.* B **38** 12 120
[17] Morinaga M, Saito J, Yukawa N and Adachi H 1990 *Acta Metall.* **38** 25
[18] Fu C L and Yoo M H 1990 *Phil. Mag. Lett.* **62** 159
[19] Woodward C, MacLaren J M and Rao S 1992 *J. Mater. Res.* **7** 1735
[20] Song Y, Tang S P, Xu J H, Mryasov O N, Freeman A J, Woodward C and Dimiduk D M 1994 *Phil. Mag.* B **70** 987
[21] Averill F W and Ellis D E 1973 *J. Chem. Phys.* **59** 6412
[22] Ellis D E, Benesh G A and Byrom E 1979 *Phys. Rev.* B **20** 1198
[23] Delley B, Ellis D E and Freeman A J 1983 *Phys. Rev.* B **27** 2132
[24] Press M R and Ellis D E 1987 *Phys. Rev.* B **35** 4438
[25] Goodman G L, Ellis D E, Alp E E and Soderholm L 1989 *J. Chem. Phys.* **91** 2983

[26] von Barth U and Hedin L 1972 *J. Phys. C: Solid State Phys.* **5** 1629
[27] Mulliken R S 1955 *J. Chem. Phys.* **23** 1833
Mulliken R S 1955 *J. Chem. Phys.* **23** 1841
Mulliken R S 1955 *J. Chem. Phys.* **23** 2338
Mulliken R S 1955 *J. Chem. Phys.* **23** 2343
[28] Brandes E A 1983 *Smithells' Metals Reference Book* 6th edn (London: Butterworth)
[29] Huang S C and Hall E L 1991 *Metall. Trans.* A **22** 2619
[30] Huang S C and Hall E L 1991 *Acta Metall. Mater.* **39** 1053
[31] Liu Y, Chen K Y, Lu G, Zhang J H and Hu Z Q 1998 *J. Mater. Res.* at press
[32] Nakamura M, Hashimoto K and Tsujimoto T 1993 *J. Mater. Res.* **8** 68
[33] Greenberg B A, Anisimov V I, Bornostirev Yu N and Taluts G G 1988 *Scr. Metall.* **22** 859
[34] Briant C L and Messmer R P 1980 *Phil. Mag.* B **42** 569
[35] Messmer R P and Briant C L 1982 *Acta. Metall.* **30** 457
[36] Briant C L and Messmer R P 1982 *Acta. Metall.* **30** 1811
[37] Wu R, Freeman A J and Olson G B 1994 *Science* **265** 376
[38] Liu Y, Chen K Y, Lu G, Zhang J H and Hu Z Q 1997 *Acta. Mater.* **45** 1851